

Article

Magnetic Iron Oxide Nanoparticles Coated by Coumarin-Bound Copolymer for Enhanced Magneto- and Photothermal Heating and Luminescent Thermometry

Alexiane Féron, Sylvain Catrouillet *, Saad Sene , Gautier Félix , Belkacem Tarek Benkhaled, Vincent Lapinte , Yannick Guari *  and Joulia Larionova *

ICGM, Univ Montpellier, CNRS, ENSCM, Montpellier, France; alexiane.feron@etu.umontpellier.fr (A.F.); saad.sene@umontpellier.fr (S.S.); gautier.felix@umontpellier.fr (G.F.);

belkacem-tarek.benkhaled@umontpellier.fr (B.T.B.); vincent.lapinte@umontpellier.fr (V.L.)

* Correspondence: sylvain.catrouillet@umontpellier.fr (S.C.); yannick.guari@umontpellier.fr (Y.G.); joulia.larionova@umontpellier.fr (J.L.)

Abstract: In this work, we report on the synthesis and investigation of new hybrid multifunctional iron oxide nanoparticles (IONPs) coated by coumarin-bound copolymer, which combine magneto- or photothermal heating with luminescent thermometry. A series of amphiphilic block copolymers, including Coum-C₁₁-PPhOx₂₇-PMOx₅₉ and Coum-C₁₁-PButOx₈-PMOx₄₂ bearing luminescent and photodimerizable coumarin moiety, as well as coumarin-free PPhOx₂₇-PMOx₅₇, were evaluated for their utility as luminescent thermometers and for encapsulating spherical 26 nm IONPs. The obtained IONP@Coum-C₁₁-PPhOx₂₇-PMOx₅₉ nano-objects are perfectly dispersible in water and able to provide macroscopic heating remotely triggered by an alternating current magnetic field (AMF) with a specific absorption rate (SAR) value of 240 W.g⁻¹ or laser irradiation with a photothermal conversion efficiency of $\eta = 68\%$. On the other hand, they exhibit temperature-dependent emission of coumarin offering the function of luminescent thermometer, which operates in the visible region between 20 °C and 60 °C in water displaying a maximal relative thermal sensitivity (S_r) of 1.53%.°C⁻¹ at 60 °C.

Keywords: nanoparticles; polymeric coating; luminescence; thermometry; coumarin



Citation: Féron, A.; Catrouillet, S.; Sene, S.; Félix, G.; Benkhaled, B.T.; Lapinte, V.; Guari, Y.; Larionova, J. Magnetic Iron Oxide Nanoparticles Coated by Coumarin-Bound Copolymer for Enhanced Magneto- and Photothermal Heating and Luminescent Thermometry.

Nanomaterials **2024**, *14*, 906. <https://doi.org/10.3390/nano14110906>

Academic Editors: Shihui Wen, Jiayan Liao and Deming Liu

Received: 29 April 2024

Revised: 16 May 2024

Accepted: 18 May 2024

Published: 22 May 2024



Copyright: © 2024 by the authors. Licensee MDPI, Basel, Switzerland. This article is an open access article distributed under the terms and conditions of the Creative Commons Attribution (CC BY) license (<https://creativecommons.org/licenses/by/4.0/>).

1. Introduction

Inorganic nanoparticles capable of inducing a macroscopic temperature increase when exposed to external *stimuli*, such as alternating current magnetic fields (AMFs) or light irradiation, have garnered significant attention for several decades. This attention stems not only from a fundamental standpoint but also due to their promising applications for hyperthermia therapy for cancer [1–3], bacterial infections [4–8], drug delivery systems [9], modulation of enzymatic reactions [10], plasmonic devices, control of single cell functions [11,12], catalytic processes [13], polymerization reactions [14] and more. A plethora of nanostructures have been engineered to serve as photothermal or magnetothermal nano-heaters, encompassing plasmonic metallic nanostructures, diverse carbon materials, metal oxides, metal alloys, semiconductors and carbides/nitrides, each offering distinct advantages for targeted heating applications [15–18]. Among these, iron oxide nanoparticles (IONPs) have been the subject of extensive investigation for many decades, owing to their exceptional capacity to generate heat when remotely exposed to external *stimuli*, their controlled size ranging from a few to hundred nanometres, different shapes, an easily functionalizable surface and biocompatibility [18–20]. Indeed, they can efficiently convert magnetic energy into heat providing an important temperature rise of colloidal solutions containing nanoparticles at macroscopic level. Recent advancements have led to the development of highly efficient IONPs with various shapes, such as spherical, cubic or dendritic

forms, achieving specific absorption rate (SAR) values of up to 1000 W g^{-1} [18,21]. More recently, IONPs have also been recognized as photothermal agents capable of providing an important temperature rise under irradiation in the near-infrared (NIR) window, making them competitive with conventional Au nano-objects [21]. Moreover, the possibility of employing them as dual magneto- and photothermal agents, therefore enhancing the heating ability by up to fivefold when compared to magnetic stimulation alone, reaching SAR values of up to 5000 W g^{-1} , has also been demonstrated [22].

One of the primary challenges in the realm of nanoparticle-assisted heating lies in achieving precise temperature control at the nanoparticle's surface. This task is especially critical due to the rapid fluctuations and localized effects inherent at such scales, necessitating innovative strategies for accurate temperature monitoring and regulation. This issue holds principal importance for optimizing various applications, including hyperthermia therapy, catalytic processes and polymerization reactions, all of which rely on maintaining specific temperature ranges or a very localized heating for optimal performance. However, conventional temperature measurement techniques, such as thermocouples or infrared thermography, often struggle with limitations in sensitivity and accuracy when applied to nanoscale systems. Fluorescence-based thermometry is emerging as one of the most promising alternative approaches, aimed at overcoming these challenges and enabling more precise local and remote temperature monitoring at the micro- and even nanoscales [23–26]. In this context, the design of multifunctional heater/luminescent thermometer nano-objects is essential for ensuring nanoparticle-assisted heating triggered by external *stimuli*, which is combined with accurate luminescent-based temperature monitoring at the nanoscale. Such design requires a careful choice of nano-heater, including its size, composition and surface functionalization, as well as the selection of appropriate luminescent probes and identification of their interface. In this line of thought, three main approaches have been implemented with IONPs. Firstly, L. D. Carlos, A. Millan and colleagues reported on the successful combination of magnetic $\gamma\text{-Fe}_2\text{O}_3$ nanoparticles with Ln^{3+} -based β -diketonate coordination complexes (where $\text{Ln}^{3+} = \text{Tb}^{3+}/\text{Eu}^{3+}, \text{Tb}^{3+}/\text{Sm}^{3+}$) as ratiometric luminescent temperature probes based on the luminescent intensity ratio of two lanthanides included into the organosilica [27] or copolymer shells [28,29]. In these works, the luminescent complexes have been encapsulated into the shells without their covalent anchoring. Secondly, both upconversion $\text{NaYF}_4:\text{Yb}^{3+}, \text{Er}^{3+}$ nanorods permitting temperature measurements based on their temperature-dependent lifetime and small IONPs allowing magnetothermal heating have been included in mesoporous silica nanoparticles [30]. This work demonstrated that the temperature inside the silica nano-objects containing magnetically activated IONPs was higher in comparison with the macroscopic ones in environmental colloidal solution. Thirdly, magnetic nanoparticles of several compositions and sizes (spherical MnFe_3O_4 of 6 nm, MnCoFeO_4 of 15 nm, spherical Fe_3O_4 nanoparticles of 12 or truncated octahedral of 25 nm) have been conjugated with organic dyes (Rhodamine B or DyLight) [12,31,32] or with fluorescent proteins, which present temperature-dependent fluorescence permitting the temperature readout [10]. Note that for these latter nano-objects, the effort has mainly been focused on the investigation of the “hot spot effect” of the nanoparticles' surface and the thermometric performance has not been investigated, except in one recent work involving Fe_3O_4 functionalized by fluorescent polymer with Rhodamine B [31]. Note also that for these multifunctional IONPs, their magnetothermal properties have been targeted and their photothermal heating has never been explored in combination with thermometry despite a significant interest in recent years in the excellent photothermal capacity of IONPs.

In this article, we report on the synthesis, magneto- and photothermal heating and luminescent thermometry of multifunctional IONPs enwrapped into amphiphilic copolymers bearing luminescent coumarin moiety. Previously, some of us demonstrated the successful coating of IONPs by a hydrophilic polymer of the polyoxazoline family [33]. The amphiphilic polymer coating has been chosen in this work because this kind of macromolecular architecture allows a good affinity with inorganic nanoparticles and ensures a dispersion of IONPs in water thanks to its hydrophilic block. Further, the polyoxazolines

are very attractive for biomedical applications because they have excellent biocompatibility, cyto- and haemocompatibility, as well as a stealth behaviour. Finally, it is expected that they can exhibit fluorescence due to their aromatic constituents [34], while, to the best of our knowledge, there have been no studies conducted on the temperature-dependent fluorescence of polyoxazolines.

Polyoxazolines can be easily synthesized by cationic ring-opening polymerization (CROP). This chemistry is a versatile tool for direct access to hydrophilic polymers using commercial 2-R-2-oxazoline monomers, where R corresponds to methyl or ethyl substituents, while hydrophobic ones result from monomers bearing propyl, butyl or phenyl substituent [35]. Hence, we elaborated two amphiphilic block copolymers, PPhOx₂₇-PMOx₅₇ and PButOx₈-PMOx₄₂, in one sequential step. Moreover, this polymerization process permits various terminal functionalizations using functional initiators and/or terminating agents. Consequently, amphiphilic block copolymers bearing a terminal coumarin unit, Coum-C₁₁-PPhOx₂₇-PMOx₅₉ and Coum-C₁₁-PButOx₈-PMOx₄₂ have been successfully prepared, as previously reported [36]. The introduction of the coumarin moiety is motivated by the following properties: (i) its ability to photodimerize under UV irradiation at 365 nm and, therefore, reinforce the IONP coating and (ii) its temperature-dependent emission in the visible region, making it a fluorescent thermometer [37]. However, although some polymers bearing a coumarin unit have already been investigated for temperature measurement purposes [38–41], they have never been used for the temperature detection and the encapsulation of nano-heaters.

In this article, a series of amphiphilic block copolymers, Coum-C₁₁-PPhOx₂₇-PMOx₅₉ and Coum-C₁₁-PButOx₈-PMOx₄₂, covalently bonded to a luminescent and photodimerizable coumarin moiety and PPhOx₂₇-PMOx₅₇ copolymer were evaluated in their micellar form as luminescent thermometers. All of them present a temperature-dependent fluorescence with the maximal relative thermal sensitivities (S_{rmax}) varying in the range 1.90–2.71%·°C⁻¹ at 60 °C. Secondly, they were tested for the encapsulation of spherical IONPs of 26 nm. The as-obtained multifunctional nano-objects IONP@Coum-C₁₁-PPhOx₂₇-PMOx₅₉ are well dispersible in water and able to provide macroscopic heating triggered either by an AMF with a specific absorption rate (SAR) value of 240 W g⁻¹ or laser irradiation with a photothermal conversion efficiency $\eta = 68\%$. Moreover, they exhibit temperature-dependent luminescence, offering the function of a luminescent thermometer, which operates in the 20–60 °C range in water displaying the S_{rmax} value of 1.53%·°C⁻¹ at 60 °C.

2. Materials and Methods

All the chemicals were purchased commercially and used without further purification. Ferric hydroxide oxide (FeO(OH) hydrated, 30–50 mesh), oleic acid (90%, OA) and oleylamine (90%, OL) were purchased from Sigma-Aldrich (Steinheim, Germany) and n-docosane (99%) was purchased from Acros organic. 2-Methyl-2-oxazoline (MOx), 2-butyl-2-oxazoline (BuOx) and 2-phenyl-2-oxazoline (PhOx) were dried and distilled from CaH₂ and stored under a dry nitrogen atmosphere (purchased from Acros organic, Geel, Belgium). Acetonitrile (ACN) was distilled before use and stored under dry nitrogen (purchased from Acros organic). 7-Hydroxy-4-methylcoumarin (97%), 11-bromoundecanol (98%), methyl p-toluenesulfonate (MeOTs) (98%), ether, chloroform, p-toluenesulfonyl chloride (TsCl, >99%), triethylamine, pyridine, piperidine, MgSO₄ and potassium carbonate were used without further purification and purchased from Acros organic.

2.1. Syntheses

Amphiphilic copolymers. The copolymers Coum-C₁₁-PPhOx_m-PMOx_n and Coum-C₁₁-PButOx_m-PMOx_n were synthesized according to already published procedures [36]. PPhOx₂₇-PMOx₅₇ was produced by using the same protocol and MeOTs as a cationic ring-opening polymerization initiator.

Formation of micelles with amphiphilic copolymers. Micelles were prepared in glass haemolysis tubes according to a film rehydration process. After weighing out approximately 20 mg of polymer, 1 mL of chloroform was added to solubilize it. CHCl_3 was chosen for solubilization as it is a good solvent for both blocks, but it is also the solvent used for nanoparticles' synthesis (later use). The solution was then evaporated using a rotary evaporator at 40 °C (pressure 104 mbar) for 1 h to obtain a thin, transparent and uniform film on the tube wall. Once the solvent was evaporated, the polymer was dried under dynamic vacuum for 3 h 30 and then under static vacuum for an additional 30 min. The film was rehydrated with an ultrapure water to achieve a concentration of 5 mg mL⁻¹. The tube was stirred for 30 min at 65 °C and then sonicated at 65 °C for 1 h. The resulting solution appears as a clear, slightly opalescent one. It should be protected from light for storage. The same protocol was followed for all the amphiphilic copolymers. The dimerization of the micelles was achieved by irradiating the sample in a cylindrical photochemical "Rayonet" reactor. It is equipped with 16 symmetrical lamps emitting at 350 nm for dimerization and 254 nm for de-dimerization.

Synthesis of pristine spherical IONPs stabilized by oleate and oleyl amine. Pristine IONPs of ca. 26 nm stabilized by oleate (OA) and by oleyl amine (OAm) were prepared by adapting a previously published thermal decomposition method (at 350 °C) by using FeO(OH) as the iron precursor in n-docosane as a solvent [42]. First, a flask containing a mixture of FeO(OH) (2.1 mmol, 0.186 g), oleic acid (10 mmol, 3.17 g) and n-docosane (5.02 g) was connected to a Schlenk line to remove moisture and oxygen for 30 min at room temperature under vacuum and magnetic stirring. Subsequently, the flask was heated to 350 °C under argon flow with a heating rate of 10 °C min⁻¹. The solution was maintained at 350 °C for a further 90 min under stirring and argon flow. Then, the mixture was cooled down to 200 °C. When the temperature reached 200 °C, the system was opened to air and the temperature was maintained at 180 °C for further 90 min to realize the nanoparticles' oxidation (from FeO to Fe₃O₄). After this period, the heating was stopped. When the temperature of the suspension reached 50 °C, cyclohexane (15 mL) was added. The obtained nanoparticles were washed twice by dispersing in diethyl ether, followed by precipitation with ethanol (1:1 v/v), and were then recovered using centrifugation (20,000 rpm, 10 min). Oleylamine (200 µL) was added to the collected material as additional stabilizer. The resultant oleate/oleylamine-coated IONP/OA/OAm nanoparticles were dispersed and stored in chloroform (15 mL) [43].

Encapsulation of IONPs by amphiphilic copolymers. The encapsulation of IONPs by amphiphilic copolymers follows a similar protocol to the formation of micelles alone, except that a balloon is used instead of glass haemolysis tubes. After weighing out the 20 mg of polymer, 1 mL of a 1 mg mL⁻¹ solution of IONPs in chloroform is added. Evaporation and vacuum drying were carried out in the same way as for the micelles alone. After the vacuum ramp, ultrapure water is added. Due to the magnetism of the IONPs, there is no need for an initial magnetic stirring step. The container is directly sonicated at 65 °C for around 1 h, alternating with vortexing to help solubilize the film. The obtained IONP@Coum-C₁₁-PPhO_{x27}-PMO_{x59} nanoparticles were washed three times with water. The nanoparticles were separated from nanoparticle-free micelles by using magnetic separation with a NdFeB- magnet (1 T).

2.2. Physical Methods

For transmission electron microscopy (TEM), 5 µL of suspension was deposited on a carbon-coated 300 mesh grid for 1 min, blotted dry by touching with a filter paper and then placed on a 2% uranyl acetate solution drop. After 1 min, the excess stain was removed by touching the edge with a filter paper, and the grid was dried at room temperature for a few min and examined using a Jeol 1400 Plus Transmission Electron Microscope (JEOL, Akishima, Japan) operating at 100 kV accelerating voltage. Data were collected with a high-sensitivity sCMOS JEOL Matataki Flash camera (JEOL, Akishima, Japan). Hydrodynamic diameter and polydispersity index (PDI) were measured using a Zetasizer

NanoZS apparatus (Malvern Panalytical B.V., Almelo, The Netherlands) equipped with a He-Ne laser (wavelength: 633 nm) at a temperature of 25 °C and a scattering angle of 173° for detection. Size measurements were performed in water. ICP-AES analysis was performed by using a Spectro Arcos ICP (AMETEK Materials Analysis, Mahwah, NJ, USA). The samples were digested in nitric and hydrochloric acids before being diluted to obtain 10 mL of a final solution in 4% of acid.

Photoluminescence and thermometry measurements. Emission and excitation spectra were performed at room temperature (298 K) in water, using an Edinburgh FLS-920 spectrofluorometer (Edinburgh Instruments Ltd., Kirkton Campus, UK). The excitation source was a 450 W Xe arc lamp. The spectra were corrected for the detection and optical spectral response of the spectrofluorometer. Photoluminescent measurements as a function of temperature (luminescent thermometry) were performed by using the temperature setup incorporated into the Edinburgh spectrofluorometer. Emission spectra were recorded in the temperature range from 20 to 60 °C. At each temperature step, a period of 2 min was given to allow the temperature to stabilize and then 1 emission spectrum was recorded with a dwell time of 0.2 s and a step of 1 nm.

Magnetohermia. Magnetohermia experiences were realized using an alternating current magnetic field generator (UltraFlex Power Technologies, Ronkonkoma, NY, USA) at 342 kHz. The generating magnetic field is 20 mT at a frequency of 342 kHz. The samples were in liquid state (colloidal solutions) and isolated with polystyrene. The temperature of the liquid was measured using an OPTRIS PI 450 thermal camera (Optris, Berlin, Germany) and an optical fibre.

Photothermia. Photothermal experiences were realized using a laser with a wavelength of 808 nm and a surface power of 2.58 W.cm⁻². The samples were in liquid state (colloidal solutions of 600 µL) in a glass tube. The temperature of the liquid was measured using an optical fibre.

2.3. Simulations and Fitting

Magnetohermia experiments. Magnetohermia experiences were fitted using the heat equation with a thermal exchange parameter ($f(T)$) as previously reported [43]:

$$c_v \frac{dT}{dt} = P - f(T)$$

where c_v and P are the heat capacity in J/K and the heat power source in W, respectively. P is linked to the SAR by the following equation:

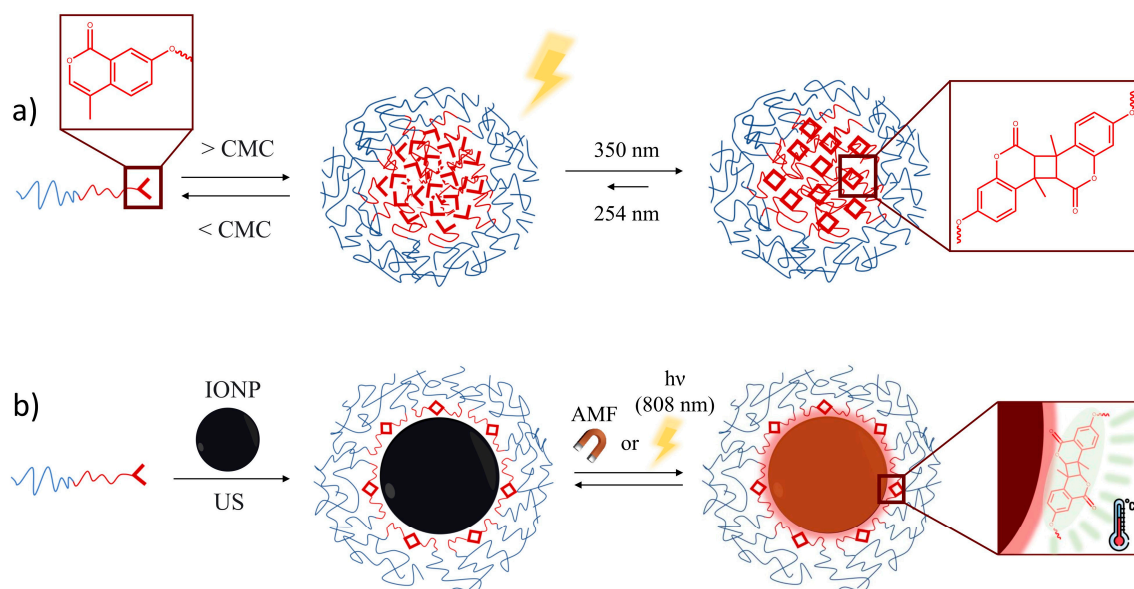
$$SAR = \frac{P}{m_{Fe}}$$

where m_{Fe} is the total mass of iron in the experiment sample.

Photothermal experiments. Photothermal experiences were fitted using a model built using COMSOL software [44]. The geometry of the experiments was reproduced in the software. The heat equation and the natural convection were solved simultaneously. The natural convection was solved for the nanoparticle suspension and for the air above the liquid. The heat equation was solved for the nanoparticle suspension, the air above and the glass tube. A thermal flux exchange was added between the glass and the rest of the environment. The thermal power source of the heat equation was calculated using the laser intensity and the shape of its spot, the light coefficient absorption a of the nanoparticle suspension and the photothermal efficiency η . The three following parameters were optimized during the fit process: the absorption, the thermal flux exchange and the thermal efficiency. The optimization of the parameters was realized using the least squares method in a python script which controls the COMSOL software.

3. Results and Discussion

The synthesis of the multifunctional nano-objects containing IONPs encapsulated by amphiphilic block copolymers was performed in three steps as follows: (i) the synthesis of a series of amphiphilic copolymers able to form micelles and the investigation of their thermometric ability (Scheme 1a), (ii) the synthesis of pristine spherical IONPs of ca. 26 nm stabilized by oleate and oleylamine and (iii) the encapsulation of IONPs by amphiphilic copolymers and the investigation of their ability to macroscopically heat their environment under external *stimuli* (light irradiation and AMF) and provide a temperature readout (Scheme 1b).

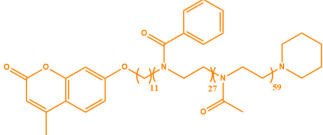
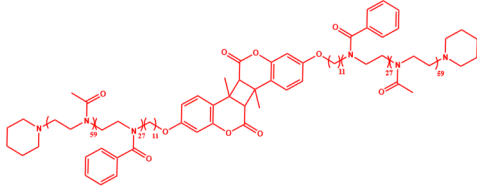
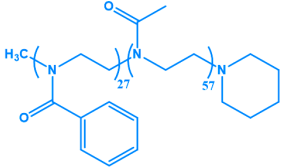
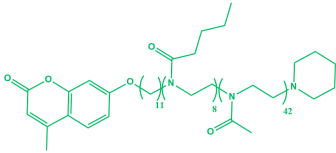
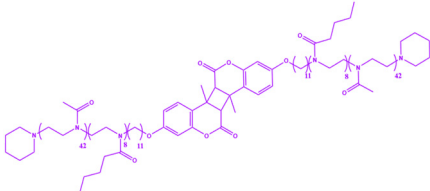


Scheme 1. Representation of the approach used in this work for (a) the preparation of micelles from amphiphilic copolymers, (b) the encapsulation of IONPs with amphiphilic copolymers in order to design multifunctional nano-objects able to provide magnetothermal or photothermal heating associated with the luminescent thermometry. CMC is the critical micellar concentration; US is the ultrasound sonication.

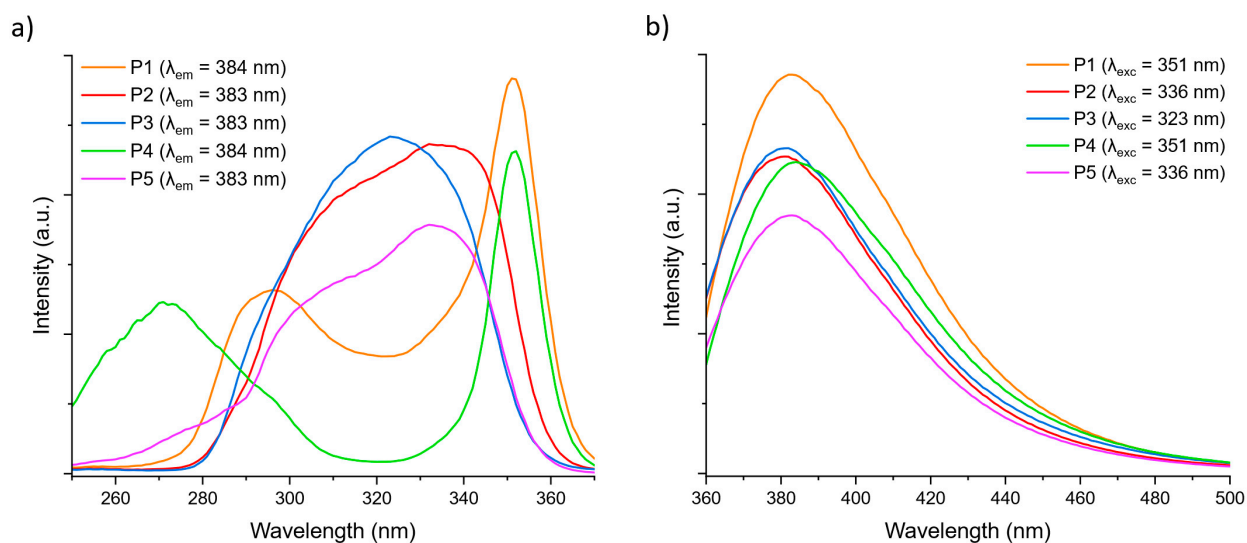
3.1. Amphiphilic Polymeric Micelles as Luminescent Thermometers

A series of amphiphilic copolymers was synthesized and investigated, with some of them functionalized by a hydrophobic and fluorescent coumarin moiety at the end of their hydrophobic block. The primary objectives were twofold: firstly, to explore their potential utility as luminescent thermometers, and secondly, to assess their suitability as luminescent shells for encapsulating hydrophobic IONPs. Each copolymer comprises a hydrophilic block of PMOx_n (where n corresponds to the number of hydrophilic repetitive units), ensuring the water dispersibility of further micelles. It was covalently bonded to a hydrophobic block denoted as PPhOx_m or PButOx_m (where m represents the number of hydrophobic repetitive units), essential for encapsulating IONPs. Two copolymers were functionalized by a coumarin moiety because the latter is fluorescent and also expected to undergo dimerization upon UV irradiation, thereby enhancing the stability of the micelles formed. Consequently, copolymer micelles containing coumarin were investigated both before and after dimerization to understand their behaviour comprehensively. Schematical representations of all the synthesized copolymers—namely, Coum- C_{11} - PPhOx_{27} - PMOx_{59} (P1 before and P2 after dimerization), PPhOx_{27} - PMOx_{57} (P3) and Coum- C_{11} - PButOx_8 - PMOx_{42} (P4 before and P5 after dimerization)—are shown in Table 1.

Table 1. Schematic representation of the amphiphilic block copolymers P1–P5 employed in this work with their excitation and emission wavenumbers.

Name	Structure	Excitation and Emission Wavelengths
Coum-C ₁₁ -PPhOx ₂₇ -PMOx ₅₉ non-dimerized (P1)		$\lambda_{exc 1} = 297 \text{ nm}$ $\lambda_{exc 2} = 351 \text{ nm}$ $\lambda_{em} = 384 \text{ nm}$
Coum-C ₁₁ -PPhOx ₂₇ -PMOx ₅₉ Dimerized (P2)		$\lambda_{exc} = 336 \text{ nm}$ $\lambda_{em} = 383 \text{ nm}$
PPhOx ₂₇ -PMOx ₅₇ (P3)		$\lambda_{exc} = 323 \text{ nm}$ $\lambda_{em} = 383 \text{ nm}$
Coum-C ₁₁ -PButOx ₈ -PMOx ₄₂ non-dimerized (P4)		$\lambda_{exc 1} = 270 \text{ nm}$ $\lambda_{exc 2} = 351 \text{ nm}$ $\lambda_{em} = 384 \text{ nm}$
Coum-C ₁₁ -PButOx ₈ -PMOx ₄₂ Dimerized (P5)		$\lambda_{exc} = 336 \text{ nm}$ $\lambda_{em} = 383 \text{ nm}$

The colour code is the same as for curves in Figure 1.

**Figure 1.** (a) Room temperature excitation spectra of a series of amphiphilic copolymers P1–P5 performed in water; (b) Room temperature emission spectra of a series of amphiphilic copolymers P1–P5 performed in water.

The amphiphilic block copolymers were prepared via a CROP process in one pot by sequential addition of the monomers using tosylate initiators. The latter included either a photosensitive coumarin modified by a C₁₁ aliphatic spacer (Coum-C₁₁-OTs) for the synthesis of Coum-C₁₁-PPhOx₂₇-PMOx₅₉ and Coum-C₁₁-PButOx₈-PMOx₄₂ copolymers [36], or a methyl group (MeOTs) for the PPhOx₂₇-PMOx₅₇. The polymerization under microwaves of hydrophobic PhOx or ButOx monomers was performed in order to obtain the hydrophobic block. Subsequently, the terminal reactive oxazolinium species of this block served as a macroinitiator to synthesize the hydrophilic PMO_x block, yielding the amphiphilic polymers. Finally, the reaction was quenched with piperidine to convert the oxazolinium end group into an unreactive terminal amine. The composition and the molecular weight of the as-obtained copolymers were determined by ¹H NMR spectroscopy (Figure S1, ESI) and GPC (Figure S2, ESI).

An amphiphilic block copolymer, Coum-C₁₁-PPhOx₂₇-PMOx₅₉, featuring a hydrophobic block of PPhOx covalently linked to the luminescent and photodimerizable coumarin moiety, was synthesized first. It is worth noting that aromatic moieties typically contribute to the fluorescence properties of organic molecules. For instance, pyrene functionalized oxazolines have already been studied for their fluorescent properties [34]. However, to the best of our knowledge, there have been no investigations of the fluorescence of commercial oxazolines and especially of a PPhOx hydrophobic block within amphiphilic block copolymers of the oxazoline family. Therefore, Coum-C₁₁-PPhOx₂₇-PMOx₅₉ could potentially combine the luminescent properties of PhOx and coumarin, along with the potential stabilization of the micelles induced by the dimerization of the latter. The formation of micelles was performed in water by solubilizing the copolymer in chloroform, followed by drying to form films, which were then rehydrated in water (Figure S3, ESI). The micelles of Coum-C₁₁-PPhOx₂₇-PMOx₅₉ could be obtained in either their dimerized or non-dimerized states by using reversible light irradiation at 350 nm for dimerization (transformation of P1 to P2) and at 254 nm for de-dimerization (transformation of P2 to P1) (Figure S4, ESI). To characterize the formed micelles, DLS measurements were performed on both the non-dimerized P1 and dimerized P2 forms. A monomodal population with a hydrodynamic diameter of 57 nm and a narrow dispersity (PDI: 0.12) was observed. The correlation and distribution curves are shown on Figure S5a,b. Notably, no significant difference in the size of the formed micelles was observed before or after dimerization. The Transmission Electronic Microscopy (TEM) image of Coum-C₁₁-PPhOx₂₇-PMOx₅₉ in its dimerized form (P2) demonstrates the presence of homogeneous spherical micelles.

In order to investigate the photoluminescence and encapsulation ability of polyoxazoline copolymer without coumarin, a block copolymer of similar composition and molar mass, PPhOx₂₇-PMOx₅₇ (P3), was synthesized and its micelles were prepared in water as described above. The DLS measurements indicated a hydrodynamic diameter of 50 nm with a narrow dispersity (PDI: 0.15) for P3 micelles (Figure S6a, ESI).

Finally, Coum-C₁₁-PButOx₈-PMOx₄₂ copolymer containing coumarin moiety, but with non-luminescent PButOx block instead of PPhOx, was synthesized and solubilized in water following the same preparation to form micelles. In this case, thanks to the presence of coumarin, micelles can also be obtained in either their dimerized or non-dimerized states by using reversible light irradiation at 350 nm for dimerization (transforming of P4 to P5) and at 254 nm for de-dimerization (transforming of P5 to P4). The DLS measurements revealed the presence of two populations, while the TEM images indicated the formation of rather cylindrical/vermicular-shaped micelles (Figure S6b,c, ESI).

The photoluminescence properties of the aqueous solutions of copolymer micelles P1–P5 were first investigated in water at room temperature. Figure 1a demonstrates their excitation spectra monitored at 383 nm. The coumarin-free copolymer PPhOx₂₇-PMOx₅₇ presents only one band in the excitation spectrum located at 323 nm. The two coumarin-containing copolymers, Coum-C₁₁-PPhOx₂₇-PMOx₅₉ and Coum-C₁₁-PButOx₈-PMOx₄₂, demonstrate the presence of two (at 297 or 270 and 351 nm) or one (at 336 nm) excitation bands depending on the non-dimerized or dimerized states of coumarin, respectively.

The emission spectra of all the copolymer micelles shown in Figure 1b indicate the occurrence of a bright luminescence at 383 or 384 nm. The emission spectrum of the coumarin-free sample P3 under an excitation at 323 nm presents the emission band at ca. 383 nm, which can be attributed to the phenyl oxazoline moiety (PhOx). The coumarin-containing copolymer Coum-C₁₁-PButOx₈-PMOx₄₂ exhibits a coumarin-linked emission at 383/384 nm in the non-dimerized (under excitation at 351 for P4) or dimerized (under excitation at 336 nm for P5) states of coumarin. Thus, the observed emission in Coum-C₁₁-PPhOx₂₇-PMOx₅₉ stems from both fluorescent species, PhOx and coumarin. The excitation and emission wavelengths are summarized in Table 1.

Second, the emission spectra of P1–P5 were investigated in the 20–60 °C temperature range in order to evaluate their potential to work as luminescent thermometers. It is noteworthy that prior studies have explored the temperature-dependent luminescence of certain polymers featuring a coumarin moiety. Notably, research on coumarin-bearing thermosensitive copolymers, based on NIPAM and oligo(ethylene glycol) methacrylate blocks, has utilized the fluorescence of coumarin for temperature detection during phase transitions [40]. Similarly, PEG and P(NIPAM)-based copolymers, incorporating the same fluorescent coumarin moiety, have been investigated for luminescent temperature detection within living cells, leveraging the fluorescence resonance energy transfer (FRET) phenomenon [41]. Additionally, reports exist on coumarin-functionalized poly(vinyl alcohol) demonstrating a linear temperature dependence of the coumarin-based emission, although temperature detection remains unexplored [39]. It is important to note, however, that the temperature-dependent fluorescence of both coumarin- and oxazolines-based copolymer micelles, as well as the determination of their thermometric parameters, have not yet been investigated.

The temperature-dependent emission spectra in the 20–60 °C temperature range are demonstrated in Figure 2 for Coum-C₁₁-PPhOx₂₇-PMOx₅₉ before (P1) and after dimerization (P2) and in Figure S7 (ESI) for the other copolymers, P3–P5. As expected, the emission intensity decreases as the temperature increases. This effect has previously been attributed to the fluorescence quenching due to the increased collision between molecules with temperature and the intersystem crossing [39]. Note that after the first heating/cooling cycle, the intensity at 20 °C perfectly coincides with that primarily obtained at 20 °C, which indicates that no photodegradation/modification of the molecules' structure occurred during the irradiation/heating. The photoluminescent intensity (integrated area between 370 and 500 nm) shows a linear temperature dependence for all the copolymers except for P4, for which a polynomial function can be used (Figure 3, Figure S8, ESI). Note that the coumarin-free copolymer P3 presents a higher intensity than P4, which offers the possibility to use it as promising luminescent temperature probe. The presence of 27 phenyl moieties for P3 instead of only one coumarin for P4 probably explains this difference.

The sensitivity of the luminescent thermometer is defined by the absolute sensitivity S_a , which can be expressed as follows:

$$S_a(T) = |\partial I(T)/\partial T| \quad (1)$$

In order to compare the sensing performance of these copolymers with other organic dye-based thermometers, the maximal relative thermal sensitivity (S_{rmax}) was calculated [23]. The S_r value refers to the relative variation rate of the thermometric parameter (I_{380} in the present systems) per degree of temperature, expressed as:

$$S_r(T) = S_a(T)/I(T) \times 100\% \quad (2)$$

The temperature dependence of S_r for P1–P5 indicates that all the S_r values are maximal at 60 °C (Figure 3, Figure S8, ESI). All the calculated S_{rmax} values are in the range 1.90–2.71%·°C⁻¹ (Table 2), which is superior to 1%·°C⁻¹, the value frequently considered as a threshold for good luminescent thermometers [24].

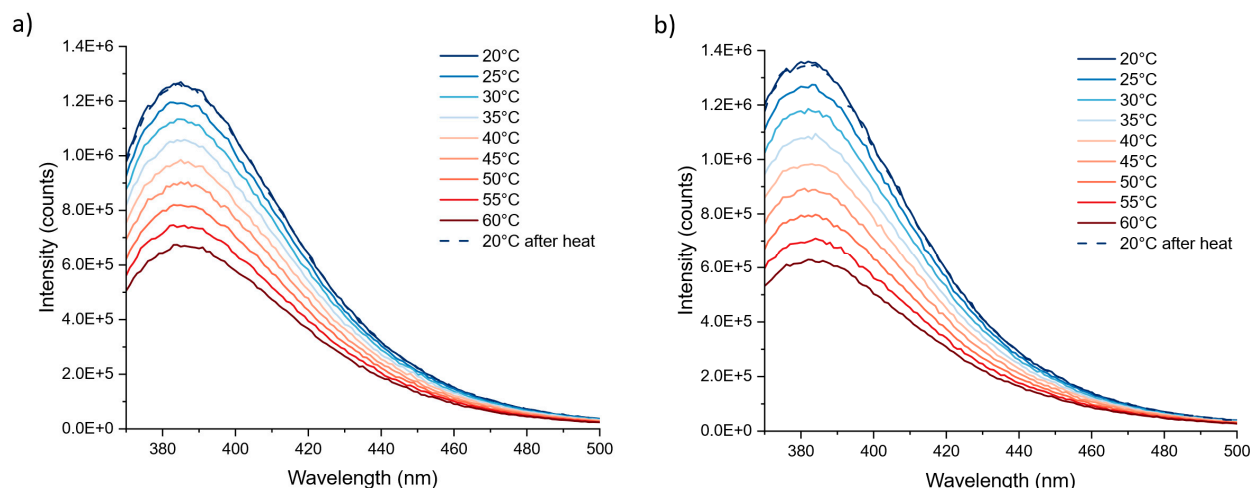


Figure 2. Emission spectra of Coum-C₁₁-PPhOx₂₇-PMOx₅₉ amphiphilic copolymer recorded in the 20–60 °C temperature range before (P1) ($\lambda_{\text{exc}} = 351$ nm) (a) and after dimerization (P2) ($\lambda_{\text{exc}} = 336$ nm) (b).

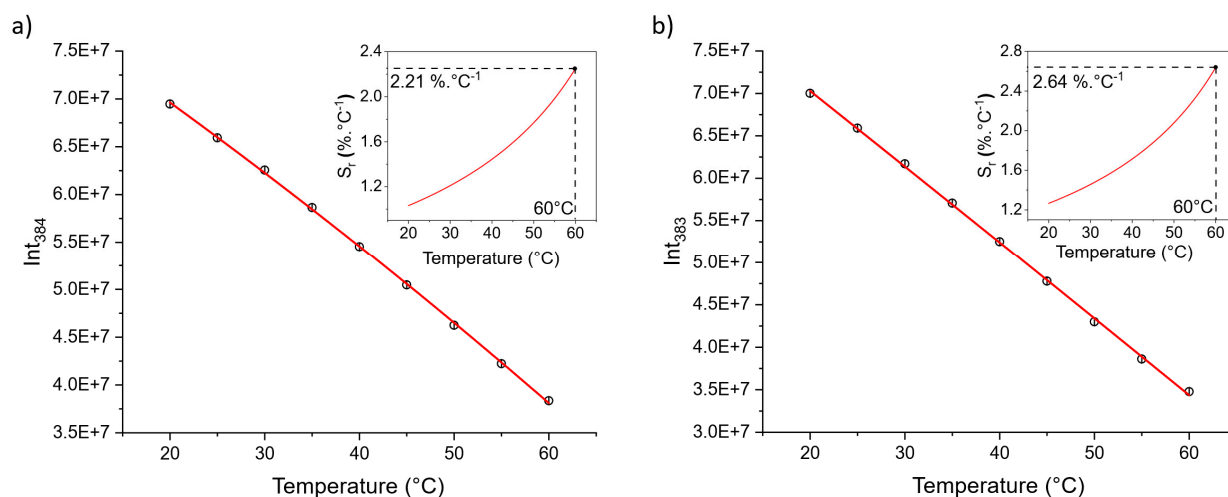


Figure 3. Temperature dependence of the main intensity, I_{385} (integrated area 370–500 nm) in the 20–60 °C temperature range in water for amphiphilic copolymers P1 (a) and P2 (b). The solid lines represent linear fits. Inset: Temperature dependence of their relative sensitivity S_r .

Table 2. Calibration parameters of the copolymer micelles P1–P5 thermometers and IONP@ Coum-C₁₁-PPhOx₂₇-PMOx₅₉ in the 20–60 °C temperature operating range.

Parameters	P1	P2	P3	P4	P5	IONP@ Coum-C ₁₁ -PPhOx ₂₇ -PMOx ₅₉
Relative maximal thermal sensitivity $S_{r\text{max}}$ (%·°C ⁻¹) at 60 °C	2.21	2.64	2.71	1.93	2.21	1.53
Uncertainty δT (°C) at 60 °C	0.28	0.40	0.87	0.14	0.29	0.82

The thermal uncertainties for copolymers P1–P5 were calculated as the smallest temperature change that can be calculated as follows:

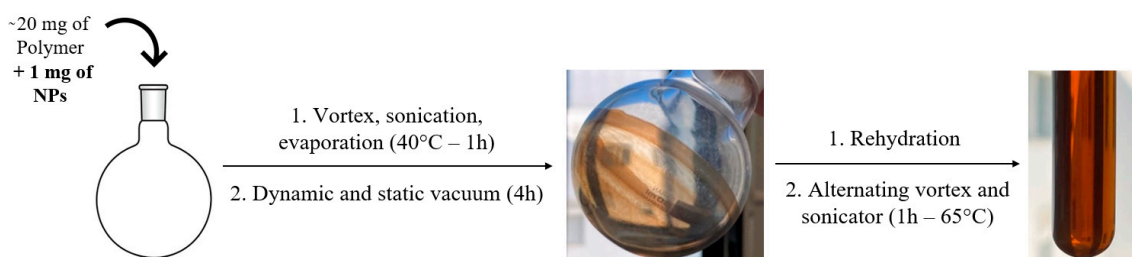
$$\delta T = \delta I / S_a(T) = \delta I / (I(T) \times S_r(T)) \quad (3)$$

The obtained thermal uncertainty values in the range 0.14–0.87 are satisfactory (Table 2). It is important to note that in Equation (3), the S_r value is in $^{\circ}\text{C}^{-1}$ and not in $\% ^{\circ}\text{C}^{-1}$.

Considering the above-described results, all the prepared copolymer micelles present a good potential as emissive thermometers and can be used for encapsulation of IONP.

3.2. IONP Coating with Amphiphilic Bloc Copolymers

The luminescent amphiphilic copolymers Coum-C₁₁-PPhOx₂₇-PMOx₅₉, Coum-C₁₁-PButOx₈-PMOx₄₂ and PPhOx₂₇-PMOx₅₇ were used for the coating of spherical IONPs of 26 nm in order to combine the thermometric function of copolymers with the magneto or photothermal heating of nanoparticles (Scheme 1b). The synthesis of the pristine IONP/OA/OAm was carried out by the classical thermal decomposition method coupled with the oxidation of FeO to Fe₃O₄ at the end of the procedure [43]. This step promotes the conversion of most of the FeO phase to Fe₃O₄. Note that the obtained nanoparticles stabilized by oleate and oleyl amine are very well dispersible in organic solvents and absolutely not dispersible in water. The encapsulation of the as-obtained IONP/OA/OAm nanoparticles by amphiphilic copolymers was carried out by using a three-step procedure, which consists of the following steps: (i) the solubilization of the IONP/OA/OAm and corresponding amphiphilic copolymer in an appropriate solvent, (ii) the formation of a film by solvent evaporation and (iii) solubilization of the film in water (Scheme 2). A first indication of the successful encapsulation of the nanoparticles by Coum-C₁₁-PPhOx₂₇-PMOx₅₉ and PPhOx₂₇-PMOx₅₇ was the complete change in behaviour in water as a homogeneous dark solution that was stable over days with no sedimentation. For Coum-C₁₁-PButOx₈-PMOx₄₂, the nanoparticles sedimented within a few minutes, which indicated that the encapsulation failed. The cylindrical morphology of these micelles probably explained the difficulties encountered for the encapsulation. After the encapsulation step, a three-time magnetic washing was performed in order to remove the encapsulated IONPs from the formed empty micelles, which do not contain IONPs. Among the tested copolymers, a successful result was obtained only with Coum-C₁₁-PPhOx₂₇-PMOx₅₉. Indeed, the nanoparticles' aggregation/sedimentation was observed after the third washing for the PPhOx₂₇-PMOx₅₇/IONP system, which indicates the total loss of copolymer during the washing procedure. On the contrary, IONP@Coum-C₁₁-PPhOx₂₇-PMOx₅₉ forms a nice colloidal aqueous solution of brown colour indicative of IONP presence. The photographs of each step of encapsulation during the formation of IONP@Coum-C₁₁-PPhOx₂₇-PMOx₅₉ nano-objects are given in Scheme 2. Note that this difference in the behaviours of Coum-C₁₁-PPhOx₂₇-PMOx₅₉ and PPhOx₂₇-PMOx₅₇ was not expected and highlights that the presence of the coumarin moiety is necessary for the IONPs' encapsulation.



Scheme 2. Scheme for IONP encapsulation with representative photographs of products obtained at each step of the procedures.

The IONP@Coum-C₁₁-PPhOx₂₇-PMOx₅₉ nano-objects were first characterized by DLS measurements, which indicated that the size of the micelles encapsulating the nanoparticles significantly increased to reach a hydrodynamic diameter of 128 nm with a narrow size distribution (PDI: 0.132) (Figure S9, ESI) in comparison with that of 57 nm (PDI: 0.120) obtained for the copolymer micelles alone (Figure S5a,b, ESI). Note that after several washing cycles, the dispersity of nanoparticles becomes much narrower (PDI: 0.132 vs. PDI: 0.246 for the first and the third washing cycles), while the hydrodynamic diameter slightly

increases (128 nm vs. 110 nm). This observation is coherent with the removal of the empty copolymer micelles during the washing. To confirm the DLS results, TEM observations were performed for the pristine IONP/OA/OAm and IONP@Coum-C₁₁-PPhOx₂₇-PMOx₅₉ nanoparticles (Figure 4). The IONP/OA/OAm nanoparticles are quasi-spherical in shape and present a size of 26 ± 2 nm (Figure S10, ESI). In TEM, the electron density is responsible for the contrast of the objects observed. Thus, in Figure 4a, the Fe₃O₄ nanoparticles appear dark due to their electronic density compared to that of the carbon support of the grid used. To obtain the TEM image depicted in Figure 4b, negative staining was employed. This consists of applying an electronically dense molecular contrast agent, which increases the image contrast by darkening the area in which it is located. The experimental protocol followed here (see Materials and Methods) makes it possible to visualize the electronically dense Fe₃O₄ nanoparticle within the micelles, which appear light in colour, the contrast agent used for the negative colouring being located around the micelles.

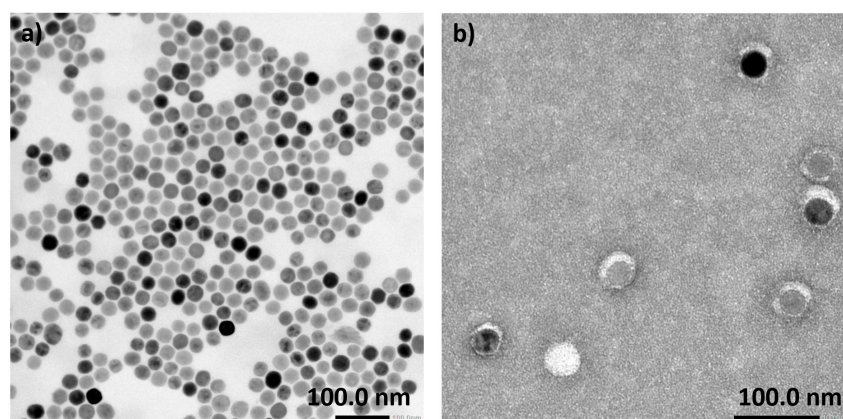


Figure 4. Transmission Electronic Microscopy images of: (a) IONP/OA/OAm, (b) IONP@Coum-C₁₁-PPhOx₂₇-PMOx₅₉ nano-objects.

3.3. Magneto- and Photothermal Heating

The magneto- and photothermal capacities of the IONP@Coum-C₁₁-PPhOx₂₇-PMOx₅₉ nanoparticles were evaluated by measuring the temperature elevation of the aqueous colloidal solutions under both an applied AMF and laser irradiation at 808 nm.

The magnetothermal properties were investigated by using a previously described home-assembled device with a 20 mT/342 kHz field [43]. Temperature elevations of $\Delta T = 10.4$ °C were observed after 15 min of exposure for an iron concentration of $0.637 \text{ mg}_{\text{Fe}} \cdot \text{mL}^{-1}$ (Figure 5a). Note that the P2 solution (free of IONPs) used as a reference here provides a temperature increase of only 1.7 °C in the same conditions. The estimation of the SAR value was performed by using a phenomenological model grounded in the Newton temperature law, incorporating a thermal exchange function (see ESI for details) [45,46]. Typically, SAR values are used to evaluate the magnetothermal performance of magnetic nanoparticles by quantifying the generated heat power under an applied AMF [18]. The energy exchange function developed with the second-order Taylor series provided the best fit for the time dependence of temperature elevation curve (Figure 5a red solid line), allowing extraction of a SAR value of $240 \pm 3 \text{ W}_{\text{Fe}} \cdot \text{g}_{\text{Fe}}^{-1}$. This value is in the range of previously published ones obtained for efficient spherical IONPs working in water [43].

The photothermal properties of the IONP@Coum-C₁₁-PPhOx₂₇-PMOx₅₉ nanoparticles were investigated in aqueous colloidal solutions under an 808 nm laser irradiation with a power of 2.58 W cm^{-2} . The temperature of the colloidal solutions was monitored by using both an optical fibre immersed in the solution and a thermal camera. An important temperature increase of $\Delta T = 13.0$ and 10.3 °C was observed under irradiation after 8 min with concentrations of 0.637 and $0.478 \text{ mg}_{\text{Fe}} \cdot \text{mL}^{-1}$, while no obvious heating effect was detected in the water without nanoparticles ($\Delta T = 0.8$ °C) (Figure 5b). The photothermal conversion efficiency, η , for the photothermal experiments was calculated by fitting the ΔT

vs. time curves for both concentrations using a model built in the COMSOL software [44]. The absorption, the thermal flux exchange and the thermal efficiency were optimized in the fitting processes. The fitting details are given in the Materials and Methods section, as well as in Figures S11–S13 (ESI). The obtained η value (for both concentrations) stands at $68 \pm 3\%$, positioning it in the higher end of values previously reported for IONPs [47].

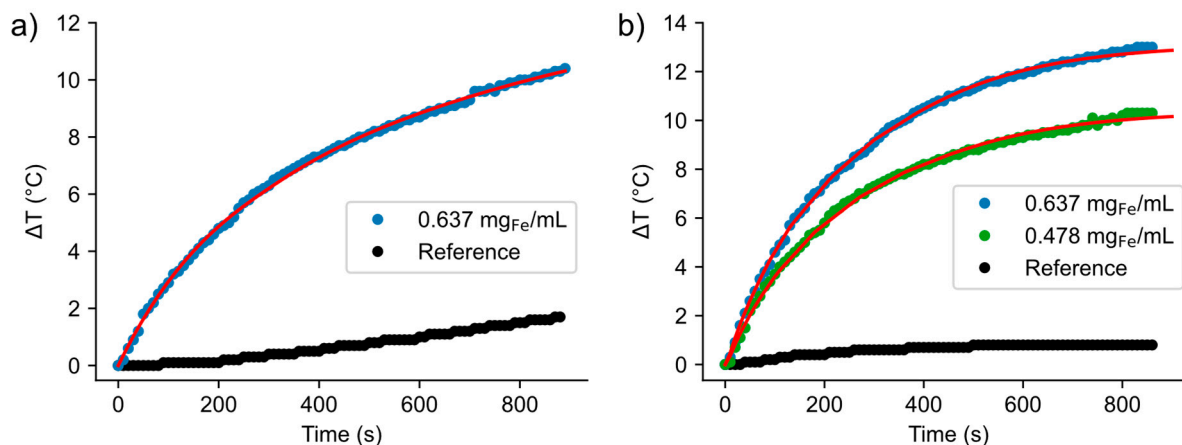


Figure 5. (a) Magnetothermal properties represented as ΔT vs. time curve measured for aqueous colloidal solution of IONP@Coum-C₁₁-PPhOx₂₇-PMOx₅₉ nanoparticles at the concentration of 0.637 mg_{Fe}·mL⁻¹ (blue circles) under an applied AMF of 20 mT/342 kHz; (b) Photothermal properties presented as ΔT vs. time curve measured for aqueous colloidal solution of IONP@Coum-C₁₁-PPhOx₂₇-PMOx₅₉ nanoparticles at the concentrations of 0.637 (blue circles) and 0.478 mg_{Fe}·mL⁻¹ (green circles) under irradiation at 808 nm (2.58 W cm⁻²). ΔT represents the difference between the temperatures of colloidal solutions of IONP@Coum-C₁₁-PPhOx₂₇-PMOx₅₉ nanoparticles and T₀ (around 20 °C). Reference is aqueous P2 solution (free of IONPs). The solid red lines represent the best fits with the second-order Taylor series model.

3.4. Luminescence and Luminescent Thermometry

The photoluminescence of the IONP@Coum-C₁₁-PPhOx₂₇-PMOx₅₉ nanoparticles was investigated in water and compared with that of the copolymer micelles of Coum-C₁₁-PPhOx₂₇-PMOx₅₉ in their non-dimerized (P1) and dimerized forms (P2). The room temperature emission spectrum of IONP@Coum-C₁₁-PPhOx₂₇-PMOx₅₉ performed in water under excitation at 323 nm exhibits a broad band at 383 nm ascribed to a Coum-C₁₁-PPhOx₂₇-PMOx₅₉-characteristic emission (Figure 6). This result indicates that despite the presence of a relatively strong absorption of IONPs in the UV region, after encapsulation, the IONP@Coum-C₁₁-PPhOx₂₇-PMOx₅₉ nanoparticles preserved the copolymer-characteristic emission, confirming successful coating with IONPs. The excitation spectrum of IONP@Coum-C₁₁-PPhOx₂₇-PMOx₅₉ displays a single band at 323 nm (Figure 6) observed before or after dimerization under UV light. In contrast, the IONP-free micelles of Coum-C₁₁-PPhOx₂₇-PMOx₅₉ show two bands at 270 nm and 351 nm in its non-dimerized form (P1) and one band at 336 nm in its dimerized (P2) state (Figure 1). This effect could be explained by the modification of the coumarin's conformation in Coum-C₁₁-PPhOx₂₇-PMOx₅₉ during the IONP coating process. Indeed, considering the fact that PPhOx₂₇-PMOx₅₇ was not able to provide stable IONP coating, we concluded that the presence of coumarin provides additional stabilization for IONP encapsulation.

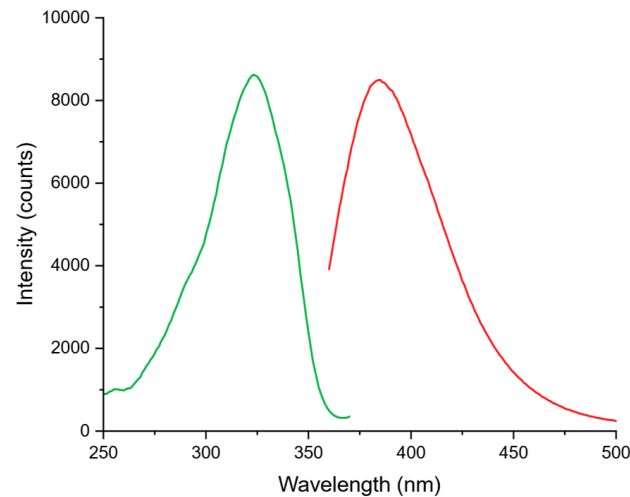


Figure 6. Excitation (green) and emission spectra (red) of aqueous colloidal solution of IONP@Coum-C₁₁-PPhOx₂₇-PMOx₅₉ nanoparticles ($\lambda_{exc} = 323$ nm, $\lambda_{em} = 383$ nm) recorded at room temperature.

Secondly, luminescence was investigated in water in the 20–60 °C temperature range in order to demonstrate the potential of these nanoparticles for temperature sensing. Figure 7a shows the temperature-dependent spectra of IONP@Coum-C₁₁-PPhOx₂₇-PMOx₅₉ under 323 nm excitation and Figure 7b demonstrates the temperature dependence of the main intensity (I_{383}) taken as an integrated area in the 370–500 nm range. The obtained intensity is linearly dependent on temperature, which confirms the possibility to use it for temperature sensing. The temperature dependence of S_r is shown in the insert in Figure 7b. The maximum on this curve (S_{rmax}) estimated from the calibration data is equal to $1.53\% \cdot ^\circ\text{C}^{-1}$ at 60 °C, which places these nanoparticles among the luminescent thermometers with a high relative thermal sensitivity ($\sim 1\% \cdot ^\circ\text{C}^{-1}$) [23]. Moreover, this value is coherent with the better S_{rmax} values obtained for nanoparticles containing luminescent thermometers based on organic dyes working in water [48]. The measured thermal uncertainty of 0.82 °C is satisfactory. The thermometric parameters for IONP@Coum-C₁₁-PPhOx₂₇-PMOx₅₉ nanoparticles are gathered in Table 2.

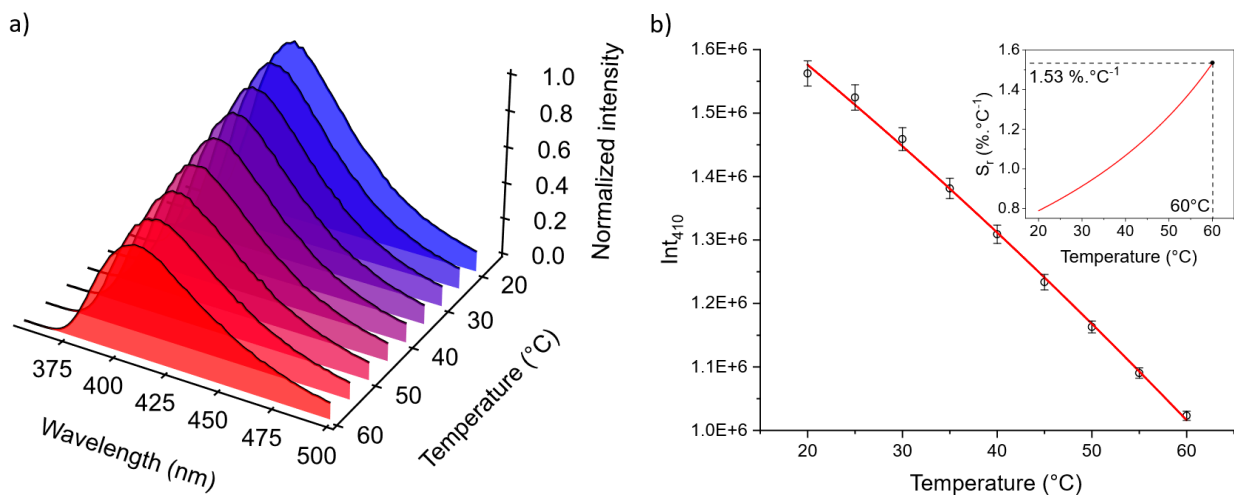


Figure 7. (a) Emission spectra of IONP@Coum-C₁₁-PPhOx₂₇-PMOx₅₉ nanoparticles ($\lambda_{exc} = 323$ nm) recorded between 20 and 60 °C; (b) Temperature dependence of the luminescent intensity with the integrated area 370–500 nm for IONP@Coum-C₁₁-PPhOx₂₇-PMOx₅₉ nanoparticles. The solid line represents a linear fitting. Inset: temperature dependence of S_r . The error bars correspond to standard error of mean determined from three consecutive temperature cycles.

4. Conclusions

In summary, in this work, we reported on the synthesis and investigation of new multifunctional heater@thermometer nano-objects obtained by coating magnetic IONPs with luminescent coumarin-bound amphiphilic copolymer and which combine magneto- or photothermal heating with luminescent thermometry. Firstly, amphiphilic coumarin and polyoxazoline-based block copolymers, Coum-C₁₁-PPhOx₂₇-PMOx₅₉ (P1 and P2 in its non- and dimerized forms) and Coum-C₁₁-PButOx₈-PMOx₄₂ (P4 and P5 in its non- and dimerized forms) copolymers, as well as a coumarin-free copolymer, PPhOx₂₇-PMOx₅₇, were synthesized and evaluated for their utility as luminescent thermometers. All of them present temperature-dependent bright luminescence at 383 nm. Their temperature-dependent luminescence is well pronounced and displays a linearity (for all except P4), making them attractive as luminescent thermometers. Their maximal relative sensitivity values (S_{rmax}) in the range 1.92–2.71%·°C⁻¹ (at 60 °C) are rather satisfactory and indicate that these copolymers can be used for efficient temperature measurements. Secondly, the capacity of these copolymers to encapsulate spherical IONPs of 26 nm was investigated. Successful encapsulation was obtained only in the case of Coum-C₁₁-PPhOx₂₇-PMOx₅₉. The as-obtained IONP@Coum-C₁₁-PPhOx₂₇-PMOx₅₉ nano-objects are well dispersible in water, while the pristine IONPs immediately aggregate in water. The TEM images demonstrate the presence of single IONP core enwrapped by a shell of copolymer. The presence of a copolymer shell is also proved by the presence of a copolymer-characteristic bright luminescence at 383 nm.

The obtained IONP@Coum-C₁₁-PPhOx₂₇-PMOx₅₉ nano-objects are able to provide a macroscopic heating triggered by an AMF with satisfactory SAR values of 240 W·g⁻¹ or by light irradiation with photothermal efficiency of 68%. On the other hand, they exhibit the temperature-dependent luminescence of a coumarin-based copolymer shell, offering the function of luminescent thermometer at 383 nm in the 20–60 °C range in water, displaying a maximal relative thermal sensitivity of 1.53%·°C⁻¹ at 60 °C.

Supplementary Materials: The following supporting information can be downloaded at: <https://www.mdpi.com/article/10.3390/nano14110906/s1>. Figure S1. ¹H NMR spectra of Coum-C₁₁-PPhOx₂₇-PMOx₅₉, Coum-C₁₁-PButOx₈-PMOx₄₂ and PPhOx₂₇-PMOx₅₇. Figure S2. GPC trace of (a) PPhOx₂₇-PMOx₅₇, (b) Coum-C₁₁-PPhOx₂₇-PMOx₅₉ and (c) Coum-C₁₁-PButOx₈-PMOx₄₂. Figure S3. Schematic representation and representative photographs for different steps in the preparation of Coum-C₁₁-PPhOx₂₇-PMOx₅₉ (P1) amphiphilic copolymer micelles. Figure S4. Schematic representation of Coum-C₁₁-PPhOx₂₇-PMOx₅₉ amphiphilic copolymer dimerization (P2) under UV irradiation. Figure S5. (a) Correlation curve and (b) Dynamic light scattering (DLS) for Coum-C₁₁-PPhOx₂₇-PMOx₅₉ amphiphilic copolymer before P1 (orange line) and after dimerization (P2) under UV irradiation (blue line), (c) TEM image for Coum-C₁₁-PPhOx₂₇-PMOx₅₉ copolymer after dimerization (P2) showing the micelle formation. Figure S6. Dynamic light scattering (DLS) for copolymers P3 (a) and P4 (b); (c) Representative TEM image for P4 showing cylindrical/vermicular shape of micelles. Figure S7. (a) Emission spectra recorded in the temperature range 20–60 °C in water for amphiphilic copolymers: (a) P3 (λ_{ex} = 323 nm), (b) P4 (λ_{ex} = 351 nm), (c) P5 (λ_{ex} = 336 nm). Figure S8. Temperature dependence of the luminescent intensity I_{384} with the integrated area 350–500 nm in the temperature range 20–60 °C for: (a) P3, (b) P4, (c) P5. The solid line represents a linear fitting. Inset: temperature dependence of S_r . Figure S9. Dynamic light scattering (DLS) measurements for IONP@Coum-C₁₁-PPhOx₂₇-PMOx₅₉ nanoparticles after the first (black curve) and the third (red curve) washing cycles. Figure S10. Size distribution for IONP/OA/OAm (n = 300). Figure S11. Simulated light density power of the 808 nm LASER used for the fit of the photothermal experiment for the 0.637 mg/mL (a) and 0.478 mg/mL (b) concentrations. Figure S12. Simulated temperature obtained during the fit of the photothermal experiment for the 0.637 mg/mL concentration at 10 s (a) and 900 s (c) and the 0.478 mg/mL concentration at 10 s (b) and 900 s (d). Figure S13. Simulated natural convection obtained during the fit of the photothermal experiment for the 0.637 mg/mL concentration at 10 s (a) and 900 s (c) and the 0.478 mg/mL concentration at 10 s (b) and 900 s (d).

Author Contributions: Conceptualization, S.C., V.L., S.S., G.F., J.L. and Y.G.; methodology, S.C., V.L., S.S., G.F., J.L. and Y.G.; validation, S.C., J.L., V.L., G.F. and S.S.; formal analysis, A.F., S.S., Y.G., B.T.B., S.C. and G.F.; investigation, A.F., S.C., G.F., S.S. and B.T.B.; resources, S.S., S.C., V.L., J.L. and Y.G.; data curation, A.F., S.S., G.F. and S.C.; writing—original draft preparation, J.L., A.F., G.F. and S.C.; writing—review and editing, S.S., G.F., V.L., J.L., S.C. and Y.G.; visualization, J.L., V.L. and Y.G.; supervision, S.S., G.F., J.L., S.C., V.L. and Y.G.; project administration, V.L., S.C., J.L. and Y.G.; funding acquisition, S.S. and S.C. All authors have read and agreed to the published version of the manuscript.

Funding: This work was supported through a Master’s student internship funding by the LabUM Chemistry of the University of Montpellier and received funding from the French State managed by the National Agency for Research under the program “Investments for the Future” (ANR-16-IDEX-0006). The work was developed within the scope of the ANR projects Killer (ANR-22-CE09-0026) and HotSpot (ANR-23-CE09-0017), the authors are grateful for funding.

Data Availability Statement: Data are contained within the article and Supplementary Materials.

Acknowledgments: Authors are grateful to the Platform of Analysis and Characterization (PAC) of ICGM for the ICP and magnetic measurements and to platform MEA at the University of Montpellier for the TEM measurements. The authors thank Basile Bouvet (ICGM) for helpful discussion.

Conflicts of Interest: The authors declare no conflicts of interest. The funders had no role in the design of the study; in the collection, analyses or interpretation of data; in the writing of the manuscript; or in the decision to publish the results.

References

1. Thiesen, B.; Jordan, A. Clinical Applications of Magnetic Nanoparticles for Hyperthermia. *Int. J. Hyperth.* **2008**, *24*, 467–474. [[CrossRef](#)] [[PubMed](#)]
2. Reddy, L.H.; Arias, J.L.; Nicolas, J.; Couvreur, P. Magnetic Nanoparticles: Design and Characterization, Toxicity and Biocompatibility, Pharmaceutical and Biomedical Applications. *Chem. Rev.* **2012**, *112*, 5818–5878. [[CrossRef](#)] [[PubMed](#)]
3. Zhu, Y.; Li, Q.; Wang, C.; Hao, Y.; Yang, N.; Chen, M.; Ji, J.; Feng, L.; Liu, Z. Rational Design of Biomaterials to Potentiate Cancer Thermal Therapy. *Chem. Rev.* **2023**, *123*, 7326–7378. [[CrossRef](#)] [[PubMed](#)]
4. de Toledo, L.d.A.S.; Rosseto, H.C.; Bruschi, M.L. Iron Oxide Magnetic Nanoparticles as Antimicrobials for Therapeutics. *Pharm. Dev. Technol.* **2018**, *23*, 316–323. [[CrossRef](#)] [[PubMed](#)]
5. Usov, N.A.; Nesmeyanov, M.S.; Tarasov, V.P. Magnetic Vortices as Efficient Nano Heaters in Magnetic Nanoparticle Hyperthermia. *Sci. Rep.* **2018**, *8*, 1224. [[CrossRef](#)] [[PubMed](#)]
6. Ibelli, T.; Templeton, S.; Levi-Polyachenko, N. Progress on Utilizing Hyperthermia for Mitigating Bacterial Infections. *Int. J. Hyperth.* **2018**, *34*, 144–156. [[CrossRef](#)] [[PubMed](#)]
7. Mahmoud, N.N.; Alkilany, A.M.; Khalil, E.A.; Al-Bakri, A.G. Nano-Photothermal Ablation Effect of Hydrophilic and Hydrophobic Functionalized Gold Nanorods on *Staphylococcus aureus* and *Propionibacterium acnes*. *Sci. Rep.* **2018**, *8*, 6881. [[CrossRef](#)] [[PubMed](#)]
8. Rodrigues, D.; Bañobre-López, M.; Espiña, B.; Rivas, J.; Azeredo, J. Effect of Magnetic Hyperthermia on the Structure of Biofilm and Cellular Viability of a Food Spoilage Bacterium. *Biofouling* **2013**, *29*, 1225–1232. [[CrossRef](#)] [[PubMed](#)]
9. Mura, S.; Nicolas, J.; Couvreur, P. Stimuli-Responsive Nanocarriers for Drug Delivery. *Nat. Mater.* **2013**, *12*, 991–1003. [[CrossRef](#)]
10. Ovejero, J.G.; Armenia, I.; Serantes, D.; Veintemillas-Verdaguer, S.; Zeballos, N.; López-Gallego, F.; Grüttner, C.; de la Fuente, J.M.; del Puerto Morales, M.; Grazu, V. Selective Magnetic Nanoheating: Combining Iron Oxide Nanoparticles for Multi-Hot-Spot Induction and Sequential Regulation. *Nano Lett.* **2021**, *21*, 7213–7220. [[CrossRef](#)]
11. Stanley, S.A.; Gagner, J.E.; Damanpour, S.; Yoshida, M.; Dordick, J.S.; Friedman, J.M. Radio-Wave Heating of Iron Oxide Nanoparticles Can Regulate Plasma Glucose in Mice. *Science* **2012**, *336*, 604–608. [[CrossRef](#)]
12. Huang, H.; Delikanli, S.; Zeng, H.; Ferkey, D.M.; Pralle, A. Remote Control of Ion Channels and Neurons through Magnetic-Field Heating of Nanoparticles. *Nat. Nanotechnol.* **2010**, *5*, 602–606. [[CrossRef](#)]
13. Marbaix, J.; Mille, N.; Lacroix, L.-M.; Asensio, J.M.; Fazzini, P.-F.; Soulantica, K.; Carrey, J.; Chaudret, B. Tuning the Composition of FeCo Nanoparticle Heating Agents for Magnetically Induced Catalysis. *ACS Appl. Nano Mater.* **2020**, *3*, 3767–3778. [[CrossRef](#)]
14. Lim, Y.; Noh, S.; Shin, T.-H.; Lee, J.; Lungerich, D.; Lee, J.-H.; Cheon, J. Magnetothermally Activated Nanometer-Level Modular Functional Group Grafting of Nanoparticles. *Nano Lett.* **2021**, *21*, 3649–3656. [[CrossRef](#)]
15. Cui, X.; Ruan, Q.; Zhuo, X.; Xia, X.; Hu, J.; Fu, R.; Li, Y.; Wang, J.; Xu, H. Photothermal Nanomaterials: A Powerful Light-to-Heat Converter. *Chem. Rev.* **2023**, *123*, 6891–6952. [[CrossRef](#)]
16. Bian, W.; Wang, Y.; Pan, Z.; Chen, N.; Li, X.; Wong, W.-L.; Liu, X.; He, Y.; Zhang, K.; Lu, Y.-J. Review of Functionalized Nanomaterials for Photothermal Therapy of Cancers. *ACS Appl. Nano Mater.* **2021**, *4*, 11353–11385. [[CrossRef](#)]
17. Ma, Z.; Mohapatra, J.; Wei, K.; Liu, J.P.; Sun, S. Magnetic Nanoparticles: Synthesis, Anisotropy, and Applications. *Chem. Rev.* **2023**, *123*, 3904–3943. [[CrossRef](#)]

18. Gavilán, H.; Avugadda, S.K.; Fernández-Cabada, T.; Soni, N.; Cassani, M.; Mai, B.T.; Chantrell, R.; Pellegrino, T. Magnetic Nanoparticles and Clusters for Magnetic Hyperthermia: Optimizing Their Heat Performance and Developing Combinatorial Therapies to Tackle Cancer. *Chem. Soc. Rev.* **2021**, *50*, 11614–11667. [[CrossRef](#)]
19. Guardia, P.; Di Corato, R.; Lartigue, L.; Wilhelm, C.; Espinosa, A.; Garcia-Hernandez, M.; Gazeau, F.; Manna, L.; Pellegrino, T. Water-Soluble Iron Oxide Nanocubes with High Values of Specific Absorption Rate for Cancer Cell Hyperthermia Treatment. *ACS Nano* **2012**, *6*, 3080–3091. [[CrossRef](#)]
20. Martínez-Boubeta, C.; Simeonidis, K.; Makridis, A.; Angelakeris, M.; Iglesias, O.; Guardia, P.; Cabot, A.; Yedra, L.; Estradé, S.; Peiró, F.; et al. Learning from Nature to Improve the Heat Generation of Iron-Oxide Nanoparticles for Magnetic Hyperthermia Applications. *Sci. Rep.* **2013**, *3*, 1652. [[CrossRef](#)]
21. de Walle, A.V.; Figuerola, A.; Espinosa, A.; Abou-Hassan, A.; Estrader, M.; Wilhelm, C. Emergence of Magnetic Nanoparticles in Photothermal and Ferroptotic Therapies. *Mater. Horiz.* **2023**, *10*, 4757–4775. [[CrossRef](#)]
22. Espinosa, A.; Di Corato, R.; Kolosnjaj-Tabi, J.; Flaud, P.; Pellegrino, T.; Wilhelm, C. Duality of Iron Oxide Nanoparticles in Cancer Therapy: Amplification of Heating Efficiency by Magnetic Hyperthermia and Photothermal Bimodal Treatment. *ACS Nano* **2016**, *10*, 2436–2446. [[CrossRef](#)]
23. Brites, C.D.S.; Balabhadra, S.; Carlos, L.D. Lanthanide-Based Thermometers: At the Cutting-Edge of Luminescence Thermometry. *Adv. Opt. Mater.* **2019**, *7*, 1801239. [[CrossRef](#)]
24. Brites, C.D.S.; Marin, R.; Suta, M.; Carneiro Neto, A.N.; Ximenes, E.; Jaque, D.; Carlos, L.D. Spotlight on Luminescence Thermometry: Basics, Challenges, and Cutting-Edge Applications. *Adv. Mater.* **2023**, *35*, 2302749. [[CrossRef](#)]
25. Bednarkiewicz, A.; Marciniak, L.; Carlos, L.D.; Jaque, D. Standardizing Luminescence Nanothermometry for Biomedical Applications. *Nanoscale* **2020**, *12*, 14405–14421. [[CrossRef](#)]
26. Jaque, D.; Vetrone, F. Luminescence Nanothermometry. *Nanoscale* **2012**, *4*, 4301–4326. [[CrossRef](#)]
27. Brites, C.D.S.; Lima, P.P.; Silva, N.J.O.; Millán, A.; Amaral, V.S.; Palacio, F.; Carlos, L.D. A Luminescent Molecular Thermometer for Long-Term Absolute Temperature Measurements at the Nanoscale. *Adv. Mater.* **2010**, *22*, 4499–4504. [[CrossRef](#)]
28. Piñol, R.; Brites, C.D.S.; Bustamante, R.; Martínez, A.; Silva, N.J.O.; Murillo, J.L.; Cases, R.; Carrey, J.; Estepa, C.; Sosa, C.; et al. Joining Time-Resolved Thermometry and Magnetic-Induced Heating in a Single Nanoparticle Unveils Intriguing Thermal Properties. *ACS Nano* **2015**, *9*, 3134–3142. [[CrossRef](#)]
29. Gu, Y.; Piñol, R.; Moreno-Loshuertos, R.; Brites, C.D.S.; Zeler, J.; Martínez, A.; Maurin-Pasturel, G.; Fernández-Silva, P.; Marco-Brualla, J.; Téllez, P.; et al. Local Temperature Increments and Induced Cell Death in Intracellular Magnetic Hyperthermia. *ACS Nano* **2023**, *17*, 6822–6832. [[CrossRef](#)]
30. Dong, J.; Zink, J.I. Taking the Temperature of the Interiors of Magnetically Heated Nanoparticles. *ACS Nano* **2014**, *8*, 5199–5207. [[CrossRef](#)]
31. Castellanos-Rubio, I.; Barón, A.; Luis-Lizarraga, O.; Rodrigo, I.; de Muro, I.G.; Orue, I.; Martínez-Martínez, V.; Castellanos-Rubio, A.; López-Arbeloa, F.; Insausti, M. Efficient Magneto-Luminescent Nanosystems Based on Rhodamine-Loaded Magnetite Nanoparticles with Optimized Heating Power and Ideal Thermosensitive Fluorescence. *ACS Appl. Mater. Interfaces* **2022**, *14*, 50033–50044. [[CrossRef](#)]
32. Davis, H.C.; Kang, S.; Lee, J.-H.; Shin, T.-H.; Putterman, H.; Cheon, J.; Shapiro, M.G. Nanoscale Heat Transfer from Magnetic Nanoparticles and Ferritin in an Alternating Magnetic Field. *Biophys. J.* **2020**, *118*, 1502–1510. [[CrossRef](#)]
33. Venturini, P.; Fleutot, S.; Cleymand, F.; Hauet, T.; Dupin, J.-C.; Ghanbaja, J.; Martinez, H.; Robin, J.-J.; Lapinte, V. Facile One-Step Synthesis of Polyoxazoline-Coated Iron Oxide Nanoparticles. *ChemistrySelect* **2018**, *3*, 11898–11901. [[CrossRef](#)]
34. Chen, C.-H.; Niko, Y.; Konishi, G. Amphiphilic Gels of Solvatochromic Fluorescent Poly(2-Oxazoline)s Containing D- π -A Pyrenes. *RSC Adv.* **2016**, *6*, 42962–42970. [[CrossRef](#)]
35. Guillerm, B.; Monge, S.; Lapinte, V.; Robin, J.-J. How to Modulate the Chemical Structure of Polyoxazolines by Appropriate Functionalization. *Macromol. Rapid Commun.* **2012**, *33*, 1600–1612. [[CrossRef](#)]
36. Belkhir, K.; Cerlati, O.; Heaugwane, D.; Tosi, A.; Benkhaled, B.T.; Brient, P.-L.; Chatard, C.; Graillet, A.; Catrouillet, S.; Balor, S.; et al. Synthesis and Self-Assembly of UV-Cross-Linkable Amphiphilic Polyoxazoline Block Copolymers: Importance of Multitechnique Characterization. *Langmuir* **2022**, *38*, 16144–16155. [[CrossRef](#)]
37. Mao, D.; Liu, X.; Qiao, Q.; Yin, W.; Zhao, M.; Cole, J.M.; Cui, J.; Xu, Z. Coumarin 545: An Emission Reference Dye with a Record-Low Temperature Coefficient for Ratiometric Fluorescence Based Temperature Measurements. *Analyst* **2015**, *140*, 1008–1013. [[CrossRef](#)]
38. Hu, X.; Li, Y.; Liu, T.; Zhang, G.; Liu, S. Responsive Polymer-Based Multicolor Fluorescent Probes for Temperature and Zn²⁺ Ions in Aqueous Media. *Sci. China Chem.* **2014**, *57*, 615–623. [[CrossRef](#)]
39. Wang, B.; Guan, X.; Hu, Y.; Su, Z. Preparation and Fluorescent Properties of Poly(Vinyl Alcohol) Bearing Coumarin. *Polym. Adv. Technol.* **2007**, *18*, 529–534. [[CrossRef](#)]
40. Inal, S.; Kölsch, J.D.; Chiappisi, L.; Kraft, M.; Gutacker, A.; Janietz, D.; Scherf, U.; Gradziński, M.; Laschewsky, A.; Neher, D. Temperature-Regulated Fluorescence Characteristics of Supramolecular Assemblies Formed by a Smart Polymer and a Conjugated Polyelectrolyte. *Macromol. Chem. Phys.* **2013**, *214*, 435–445. [[CrossRef](#)]
41. Hu, X.; Li, Y.; Liu, T.; Zhang, G.; Liu, S. Intracellular Cascade FRET for Temperature Imaging of Living Cells with Polymeric Ratiometric Fluorescent Thermometers. *ACS Appl. Mater. Interfaces* **2015**, *7*, 15551–15560. [[CrossRef](#)]

42. Yu, W.W.; Falkner, J.C.; Yavuz, C.T.; Colvin, V.L. Synthesis of Monodisperse Iron Oxide Nanocrystals by Thermal Decomposition of Iron Carboxylate Salts. *Chem. Commun.* **2004**, 2306–2307. [[CrossRef](#)]
43. Bouvet, B.; Sene, S.; Félix, G.; Havot, J.; Audran, G.; Marque, S.R.A.; Larionova, J.; Guari, Y. Cascade Strategy for Triggered Radical Release by Magnetic Nanoparticles Grafted with Thermosensitive Alkoxyamine. *Nanoscale* **2022**, *15*, 144–153. [[CrossRef](#)]
44. COMSOL® Software Version 6.0 Release Highlights. Available online: <https://www.comsol.com/release/6.0> (accessed on 18 April 2024).
45. Wildeboer, R.R.; Southern, P.; Pankhurst, Q.A. On the Reliable Measurement of Specific Absorption Rates and Intrinsic Loss Parameters in Magnetic Hyperthermia Materials. *J. Phys. D Appl. Phys.* **2014**, *47*, 495003. [[CrossRef](#)]
46. Lanier, O.L.; Korotych, O.I.; Monsalve, A.G.; Wable, D.; Savliwala, S.; Grooms, N.W.F.; Nacea, C.; Tuitt, O.R.; Dobson, J. Evaluation of Magnetic Nanoparticles for Magnetic Fluid Hyperthermia. *Int. J. Hyperth.* **2019**, *36*, 687–701. [[CrossRef](#)]
47. Roca, A.G.; Lopez-Barbera, J.F.; Lafuente, A.; Özel, F.; Fantechi, E.; Muro-Cruces, J.; Hémadi, M.; Sepulveda, B.; Nogues, J. Iron Oxide Nanoparticles (Fe_3O_4 , $\gamma\text{-Fe}_2\text{O}_3$ and FeO) as Photothermal Heat Mediators in the First, Second and Third Biological Windows. *Phys. Rep.* **2023**, *1043*, 1–35. [[CrossRef](#)]
48. Qin, T.; Liu, B.; Zhu, K.; Luo, Z.; Huang, Y.; Pan, C.; Wang, L. Organic Fluorescent Thermometers: Highlights from 2013 to 2017. *TrAC Trends Anal. Chem.* **2018**, *102*, 259–271. [[CrossRef](#)]

Disclaimer/Publisher’s Note: The statements, opinions and data contained in all publications are solely those of the individual author(s) and contributor(s) and not of MDPI and/or the editor(s). MDPI and/or the editor(s) disclaim responsibility for any injury to people or property resulting from any ideas, methods, instructions or products referred to in the content.